Glacier Image Velocimetry: an open-source toolbox for easy and rapid calculation of high-resolution glacier-velocity fields

Maximillian Van Wyk de Vries[1,2] and Andrew D. Wickert[1,2]

[1]Department of Earth & Environmental Sciences, University of Minnesota, Minneapolis, MN
[2]Saint Anthony Falls Laboratory, University of Minnesota, Minneapolis, MN
Correspondence: Maximillian Van Wyk de Vries (vanwy048@umn.edu)

Abstract. We present 'Glacier Image Velocimetry' (GIV), an open-source and easy-to-use software toolkit for rapidly calculating high spatial resolution glacier-velocity fields. Glacier ice velocity fields reveal flow dynamics, ice-flux changes, and (with additional data and modelling) ice thickness. Obtaining glacier-velocity measurements over wide areas with field techniques is labour intensive and often a safety risk. Recent increased availability of high-resolution, short-repeat-time optical imagery allow us to obtain ice displacement fields using 'feature tracking' based on the presence of persistent irregularities on the ice surface, and hence, velocity over time. GIV is fully parallelized, and automatically detects, filters, and extracts velocities from large datasets of images. Through this coupled toolchain and an easy-to-use GUI, GIV can rapidly analyze hundreds to thousands of image pairs on a laptop or desktop computer. We present four example applications of the GIV toolkit in which we complement a glaciology field campaign (Glaciar Perito Moreno, Argentina) and calculate the velocity fields of small (Glacier d'Argentière, France) and very large (Vavilov ice cap, Russia) glaciers as well as a tropical ice cap (Volcán Chimborazo, Ecuador). Fully commented MATLAB code and a standalone app for GIV are available from GitHub and Zenodo at github.com/MaxVWDV/glacier-image-velocimetry.

1 Introduction

Satellite imagery revolutionized our ability to study changes on the surface of our planet. Satellite datasets now routinely support storm and drought evaluations (Klemas, 2009; Rhee et al., 2010; AghaKouchak et al., 2015), volcanic activity monitoring (Wright et al., 2002; Harris, 2013), and landslide-hazard analysis (Metternicht et al., 2005; Tralli et al., 2005; Marc and Hovius, 2015). In glaciology, remote sensing has enabled global glacier inventories (Pfeffer et al., 2014; Earl and Gardner, 2016) as well as high-resolution elevation models and image mosaics of the Antarctic and Greenland ice sheets (Bindschadler et al., 2008; Hui et al., 2013; Howat et al., 2014; Porter et al., 2018). With temperatures consistently rising throughout much of the globe, these images also provide an important temporal record of changes in ice extent and volume, as well as an effective tool for communicating these changes to the broader public (Scambos et al., 2007; Stocker et al., 2013; Howat et al., 2019).

The use of imagery is not limited to mapping changes in glacial extent. The snowline on temperate glaciers, easily visible from end-of-melt-season images, defines the equilibrium-line altitude, thereby delineating glacier accumulation and ablation areas (Bamber and Rivera, 2007; Rabatel et al., 2008; Yuwei et al., 2014). Identifying both seasonal and annual changes in snowline can provide important information about local winter precipitation, summer air temperatures, and longer-term glacier mass changes (Bakke and Nesje, 2011).

Velocity measurements permit scientists to map glacier divides and drainage basins (Davies and Glasser, 2012; Pfeffer et al., 2014; Mouginot and Rignot, 2015) and track changes in surface melt production and accumulation (Mote, 2007; Sneed and Hamilton, 2007). Advancing techniques to remotely sense glaciers – and particularly their velocities – continues to provide new avenues to address key questions in ice dynamics and the future of glaciers under a changing climate (Stearns et al., 2008; Wal et al., 2008; Rignot et al., 2011; Willis et al., 2018). Even the earliest glaciologists identified that glaciers may flow as viscous fluids (Forbes, 1840, 1846; Bottomley, 1879; Nye, 1952), and later that glacier-surface motions reflect a complex interplay between internal deformation, basal sliding, and deformation of subglacial sediments (Deeley and Parr, 1914; Weertman, 1957; Kamb and LaChapelle, 1964; Nye, 1970; Fowler, 2010). Sudden peaks in velocity may result from a sudden change in basal sliding, perhaps as the result of changing englacial hydrology. Long-term speedups or slowdowns may reflect climatic shifts or drainage reorganizations.

Deriving glacier velocities from satellite imagery is possible through an image-analysis technique known as 'feature tracking', 'image cross correlation', or 'particle image velocimetry'. The latter term, 'particle image velocimetry', describes a well-established technique in fluid dynamics, typically involving the use of a high-speed digital camera to track the motion of tracers within a fluid in a laboratory setting (Buchhave, 1992; Grant, 1997; Raffel et al., 2018) . These ideas were first carried over to the field of glaciology by Bindschadler and Scambos (1991) and Scambos et al. (1992) to evaluate the flow velocity of a portion of an Antarctic ice stream. Since that time, the increasing abundance and availability of imagery has facilitated expanded use of feature-tracking-based velocimetry techniques. With the release of the full Landsat data archive and launch of Sentinel-2, 10–30-m pixel resolution imagery of any given location is now available at sub-weekly repeat coverage intervals. A number of studies apply this exceptional archive to map velocity fields across the major ice sheets as well those of many glaciers around the world (Gardner et al., 2018; Millan, 2019).

Prior to the advent of remote sensing, spatially distributed measurements of glacier flow velocities required lengthy field campaigns (Meier and Tangborn, 1965; Hooke et al., 1989; Chadwell, 1999; Mair et al., 2003). Nowadays full 2D flow-velocity maps may be readily calculated from a variety of optical and radar-based satellite imagery (Heid and Kääb, 2012b; Fahnestock et al., 2016). For this toolbox we focus on optical imagery products due to their ease of access, limited need for pre-processing and high spatial and temporal resolution (Drusch et al., 2012; Heid and Kääb, 2012b, a; Kääb et al., 2016; Darji et al., 2018).

A number of tools exist to derive displacements from imagery, as partially reviewed by Heid and Kääb (2012a); Jawak et al. (2018) and Darji et al. (2018). In addition, near-global ice-velocity maps are calculated in near-real time from Landsat and other freely available satellite data sources (Scambos, 2016; Gardner et al., 2020). Table 1 presents a non-exhaustive list of software packages available online. Our objective with the 'Glacier Image Velocimetry' (GIV) toolbox presented here is to provide an

easy-to-use, flexible, and efficient tool that can derive high spatial resolution and monthly temporal resolution surface-velocity maps of any glacier. The following section will run through the basics of the image-feature-tracking techniques and advances built into GIV.

2 Methods and model setup

The fundamental idea behind feature tracking is based on techniques used to co-register images: the properties of two images are compared in order to identify the best-fit location of one image within the other (Scambos et al., 1992; Thielicke and Stamhuis, 2014; Messerli and Grinsted, 2015). In feature tracking, including in GIV, individual images are divided into a grid of smaller images (referred to as 'chips'). We compare each individual 'chip' from the first image (I1) to ~~the corresponding~~ a surrounding portion within a second image (I2), and find the best matching portion of I2. If no displacement has occurred between the two images, the best-fitting portion of I2 will have the same location as the original 'chip' on I1 (excluding any georeferencing or distortion-related errors). However, if any motion has occurred between the two images, the corresponding best matching 'chip' within I2 will be displaced relative the original location within I1. We may then determine the bulk displacement in pixels between the original I1 'chip' and best match I2 'chip'. The correlation coefficients between the original chip and surrounding area within I2 allow a Gaussian curve to be fit to this grid in order to determine the peak location at sub-pixel accuracy. Repeating this routine for every chip within the original image allows a 2D surface velocity field to be derived.

When initially developed for use in laboratory-based fluid dynamics, the camera, lighting, and tracer-particle conditions were all closely constrained (Grant, 1997; Raffel et al., 2018). On glaciers, features change over time as crevasses open and close, snow drifts, and ablation exposes new surfaces. In addition, the satellite may acquire imagery from slightly different locations and angles with each pass, and lighting conditions depend strongly on the time of day and year, as well as local weather conditions (Berthier et al., 2005; Kääb et al., 2016). This complexity raises additional problems in the use of this technique for deriving glacier velocities, and makes it entirely unusable in some cases (e.g. images too far spaced in time relative to the speed of the glacier surface for image pairs to retain any coherence). These problems can be mitigated though a combination of image pre-filtering, comparison between adjacent velocity maps, and outlier filtering. We also refer readers to chapters 2 and 4 of Altena (2018) for detailed discussion on these topics. The Glacier Image Velocimetry toolbox makes use of these ~~approaches~~methods, with a particular emphasis on noise reduction in individual velocity map outputs through the use of large datasets. Figure 1 presents the overall model setup and order of operations.

2.1 Model pre-processing

Prior to running the feature-tracking algorithms, the satellite images are first loaded into the workspace and filtered. The user interface will prompt the user to enter the coordinates of the images (minimum and maximum latitude and longitude), and to select a given folder in which the images are stored. These images can be .png, .jpg, or .geotiff files of the area, with each file name being the date of image acquisition (in yyyymmdd format). In the case of a geotiff input, GIV will automatically load the geographic information from the input. GIV will then extract the dates from the file names, calculate time between

Table 1. Non-exhaustive list of codes and toolboxes that may be used for feature tracking, and associated references. 3 = fully available, 2 = available, but relies on commercial software, 1 = not available. A spreadsheet with download links is available in the supplementary material.

Toolbox	Source	Summary	Avaliability
Auto-RIFT	Gardner et al. (2018)	Python dense feature tracking package for calculating displacement from optical or radar imagery. Used for calculating the ITS_LIVE global velocity dataset.	3
CARST	Zheng et al. (2019a)	Python and bash scripts for feature tracking and ice elevation change analysis.	3
CIAS	Kääb and Vollmer (2000)	IDL based correlation software to compute offsets between two images.	3
Cosi-Corr	Leprince et al. (2007a)	IDL/ENVI based package for image co-registration and displacement mapping.	2
EMT	Schwalbe and Maas (2017)	Workflow for analysis and feature tracking of time -lapse ground based imagery.	3
GIV	This study.	GUI based feature tracking toolbox for glaciology.	3
fourDvel	Minchew et al. (2017)	Fortran routine for calculation of 3d velocity fields from geolocated displacement data.	3
ImCorr	Scambos et al. (1992)	C and Fortran package for dense feature tracking of satellite or airphoto imagery.	3
ImGRAFT	Messerli and Grinsted (2015)	MATLAB based package for georectification of ground-based imagery and feature tracking.	2
matpiv	Sveen (2004)	MATLAB based toolbox for pattern matching and particle image velocimetry (PIV).	2
PIVlab	Thielicke and Stamhuis (2014)	GUI based MATLAB PIV toolbox	2
Pointcatcher	James et al. (2016)	MATLAB based toolbox for facilitating manual feature tracking in image time-series.	2
PyCorr	Fahnestock et al. (2016)	Python based feature tracking toolbox. Used for calculating the GoLIVE global velocity dataset.	1
PyTrx	How et al. (2020)	Python toolbox created for calculating displacements from oblique images and time-lapse image series.	3
SendIT	Nagy et al. (2019)	Flexible processing toolbox for retrieval of glacier surface velocities, based on ImCorr.	3
vmap	Shean (2019)	Ames Stereo Pipeline based image correlator for velocity map generation.	3
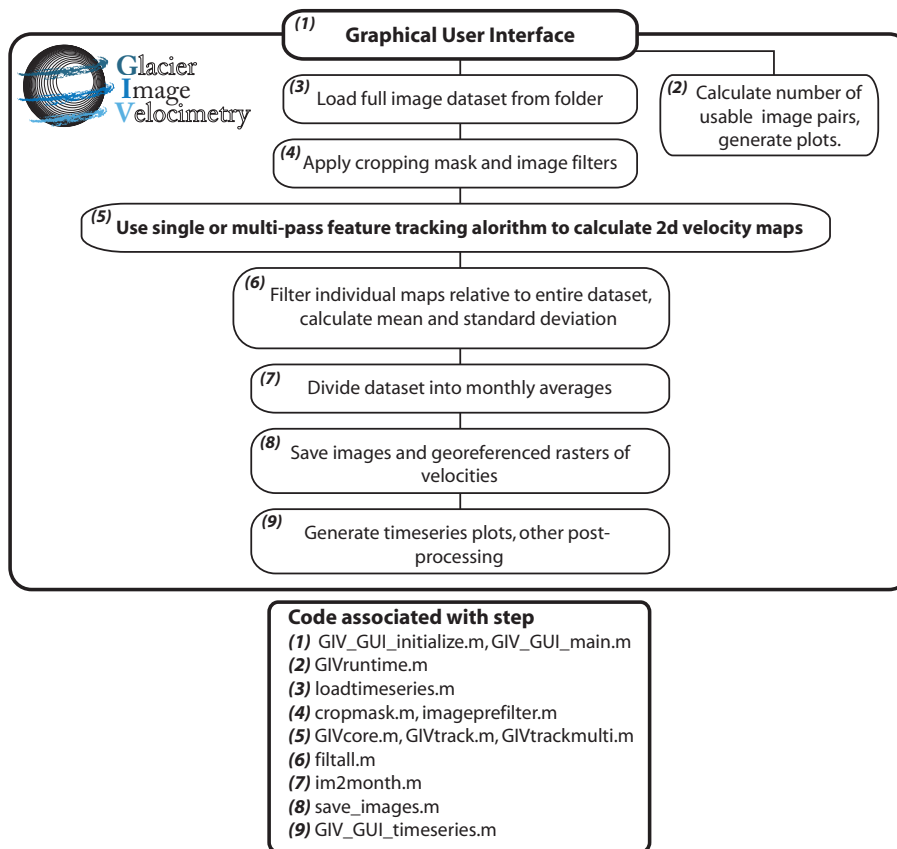
Figure 1. Flowchart describing the Glacier Image Velocimetry toolbox design. Names of the code files associated with each step are given for reference (and are available in the linked Zenodo repository). Note that users can access the source code, but that it is not necessary for running GIV. Users may enter all parameters into fields in the user interface, with subsequent steps automatically performed by the toolbox.

images, and load the raw image data into an array for further processing. The user also inputs a modified image with glaciers of interest converted to pure white (RGB 255,255,255). This image is loaded by GIV and converted into a binary mask with areas within (1) and outside (0) the computational region. The size and resolution of images are also automatically calculated and re-sampled to a common resolution, such that images from different satellites may be combined into the same dataset.

Following this, GIV filters the images ~~following~~ according to user-defined settings. GIV includes a range of filters in order to reduce the effect of unwanted noise (e.g. clouds and shadows) and emphasize trackable features (e.g. crevasses, snowdrifts, supraglacial debris). In particular we include high-pass, Sobel, and Laplacian filter options to emphasize short-wavelength features and edges, as well as intensity-capping and contrast-limited histogram-equalization filters to improve image contrast (Sveen, 2004; Thielicke and Stamhuis, 2014; Gardner et al., 2018). We also ~~developed a~~ include a variation of the orientation

filter (Fitch et al., 2002) named 'near anisotropic orientation filter' (NAOF), ~~which in most cases produces the highest number of correctly tracked velocity 'chips'~~. We define this filter as:

$$I_f = \sum_{i=1}^{4} \cos\left[\arctan 2(I_o * \alpha_i, I_o * R[\alpha_i])\right] \tag{1}$$

With I_f the filtered image, I_o the original image, α representing four different convolution matrices oriented at 45 degrees from each other using the 8 adjacent pixels, ~~Re[x] representing the real portion of complex number x,~~ $\arctan 2(x,y)$ representing the four-quadrant arctangent (also called the two-argument arctangent), $x * y$ representing a two dimensional matrix convolution, and $R[x]$ representing a 90 degree matrix rotation. This filter works by summing differently angled orientation filters together in order to recover a 'pseudo-feature' with the same location as the original feature, but with an increased contrast between the feature and the background, and homogenized magnitude (Fitch et al., 2002; Kobayashi and Otsu, 2008). Information on absolute pixel color magnitude is discarded, with only information on color gradients preserved. A similar result may be obtained by convolving the original image with a single ~~symmetrical convolution matrix~~ convolution matrix summing the four directional filters, but this ~~also~~ normalizes all features to a single magnitude and results in a larger number of false matches. The NAOF has the advantages of (a) strongly increasing the contrast between features and background; (b) removing contrast differences between clouded, shadowed, and clear areas; and (c) preserving feature location and uniqueness. Figure 2 shows examples of how this filter is able to recover features from ~~otherwise unusable~~ challenging images. Many glaciated areas remain ~~partially~~ cloud covered and shadowed for much of the year, so being able to recover partial velocity fields from these images can greatly increase the size of potential datasets. Note that no amount of filtering can improve certain images, such as those in which cloud cover is too thick for the glacier surface to be visible. An evaluation of the quality of velocity maps derived from different image filters is provided in the supplementary material (figures S1-S16). These show that NAOF~~filtered images generally provide velocity maps with the highest signal to noise ratio, and that~~, contrast-limited histogram-equalization and high-pass filtering ~~also provide an~~ provide a major improvement over raw imagery.

2.2 Velocity calculations

The central part of any feature tracking code involves matching a small region of one image ('chip') with a surrounding region of a second image ('search area'). The 'chip' is matched to the 'search area' through two-dimensional cross correlation, which may be performed in the spatial or frequency domain (Thielicke and Stamhuis, 2014; Altena, 2018). Matching in the spatial domain ('normalized cross correlation') may better account for feature distortion or shear, and may have a higher accuracy (Thielicke and Stamhuis, 2014). Frequency domain methods ('frequency cross correlation') generally benefit from a greater computational efficiency, as the correlation matrix is calculated across the whole domain in one operation. We implement frequency-domain matching in GIV, as feature distortion is minimal in most glaciers and it has been found to perform well in prior studies (e.g., Heid and Kääb, 2012a). We refer readers to Thielicke and Stamhuis (2014) and chapter 4 of Altena (2018) for more details on these topics.

Frequency cross correlation involves calculating the correlation between the 'chip' and 'search area' in the frequency domain. This is done by converting both the 'chip' and 'search area' to the frequency domain using a fast Fourier transform (FFT), calculating the pointwise product between these two matrices and converting the resulting similarity matrix back to the spatial domain with an inverse FFT (IFFT). This step is repeated on each chip within the original image, and is the most computationally expensive of the entire process.

Displacements may be derived from an image pair either with a single pass across the images, or with multiple passes with gradually reducing window sizes (Thielicke and Stamhuis, 2014; Raffel et al., 2018). Single-pass methods generally have the advantage of generally being faster at coarse resolutions and are less at risk of smearing one erroneous value over a larger area. Multi-pass methods update displacement estimates over multiple iterations, refining initial coarse-window-size displacement calculations using progressively smaller window sizes. Multi-pass methods combine the advantages of better feature matching at large window sizes with the higher spatial resolution of small window sizes. Both methods are integrated into GIV, with a single-pass method based on ImGRAFT (Messerli and Grinsted, 2015) and a 3-iteration multi-pass algorithm modified from matpiv (Sveen, 2004). Both functions have been tested in a number of previous studies, with matpiv being used extensively in fluid-dynamics research (e.g., Sveen and Cowen, 2004; Sveen, 2004; Lee et al., 2017; Oertel and Süfke, 2020).

Comparison between raw optical images, band-summed images and NAOF-filtered images for a clear image (a, d, g), a heavily shadowed image (b, e, h), and a cloudy image (c, f, i). Note how despite the complexity, the NAOF images recover a clear and easily traceable feature pattern on the surface of the glacier that is suitable for obtaining velocities. The shadow line leaves an artefact in h, but is a marked improvement on the lack of features in the shaded area in e. Images from Sentinel-2.

The core of both the single- and multi-pass methods involves converting each image chip to the frequency domain using a fast Fourier transform (FFT) algorithm, calculating the correlation coefficient with surrounding areas within a given search window, and converting the resulting similarity matrix back to the spatial domain with an inverse FFT (IFFT). This step is repeated on each chip within the original image, and is the most computationally expensive of the entire process.

Chip matching may also be performed in the spatial domain, where it is known as 'normalized' cross correlation. Spatial domain matching may better account for shear or distortion of features, but loses the computational efficiency of frequency-domain matches. We implement frequency-domain matching in GIV, as feature distortion is minimal in most glaciers. We refer readers to Thielicke and Stamhuis (2014) and chapter 4 of Altena (2018) for more details. An experiment evaluating the difference between a normalized cross correlation algorithm and the multipass frequency domain cross correlation in GIV is given in the supplementary material. We find that the multipass frequency domain algorithm produces velocity maps with higher signal to noise ratio than the normalized cross correlation algorithm across test scenarios with and without a range of cloud cover.

GIV is written in MATLAB. Despite being a high-level interpreted programming language, MATLAB performs FFT calculations using precompiled C and Fortran bindings for the FFTW library (Frigo and Johnson, 1998, 2005). Due to this being the rate-limiting step in feature tracking calculations (>90% of computation time in most cases), such code may be written in MATLAB with few performance issues relative to other programming languages.

As the feature-tracking correlation between two images inherently requires a large number of FFT and IFFT operations, this step has limited potential for further optimization. Computation time may instead be decreased by deriving displacement fields
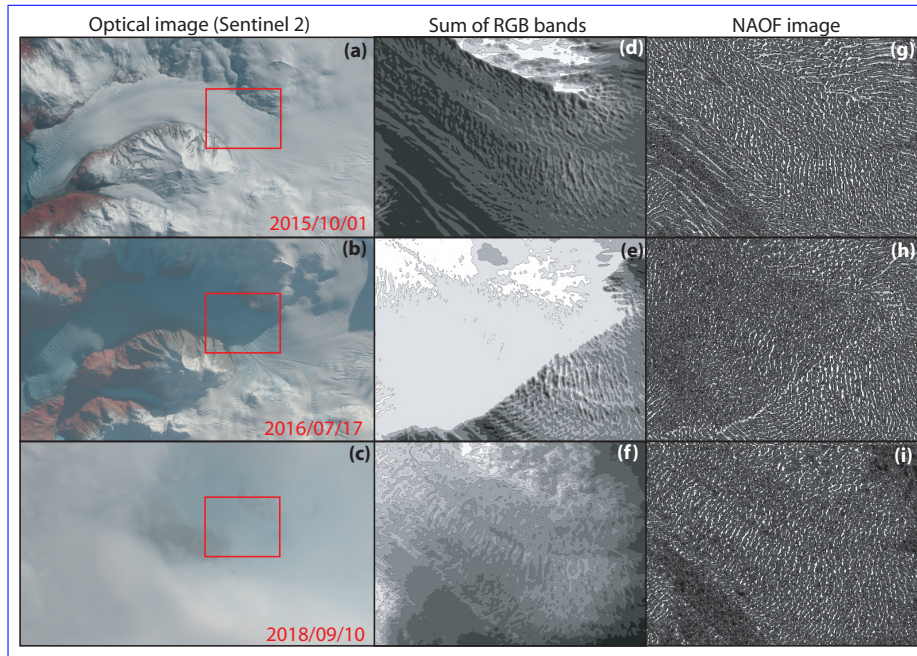
Figure 2. Comparison between raw optical images, band-summed images and NAOF-filtered images for a clear image (a, d, g), a heavily shadowed image (b, e, h), and a cloudy image (c, f, i). Note how despite the complexity, the NAOF images recover a clear and easily traceable feature pattern on the surface of the glacier that is suitable for obtaining velocities. The shadow line leaves an artefact in h, but is a marked improvement on the lack of features in the shaded area in e. Images from Sentinel-2.

165 from different image pairs in parallel rather than in series. This requires a slightly different code design: First, GIV detects the number of physical cores on the user's computer and starts a parallel pool (users may also start their own parallel pool with a chosen number of cores). It then decomposes the full sequence of image pairs into sub-sequences the size of the number of cores. Finally, it distributes each sub-sequence across the cores in the computer to be computed in parallel. Figure 3 shows the increase in computation speed with number of cores used in different scenarios. This enables large datasets to be processed

170 more rapidly, even on standard laptop and desktop computers.

GIV may also calculate velocity maps for pairs of non-consecutive images, which we refer to as "temporal oversampling", resulting in much larger final datasets. The user inputs maximum and minimum temporal separations for image pairs, and GIV extracts all suitable pairs, including those that are not consecutive. For a dataset of n images, this theoretically enables a total of $(n^2 - n)/2$ image pairs. (For example, this would produce 19,900 image pairs from a 200-satellite-image time-series). For

175 heavily clouded datasets this also has the advantage of increasing the likelihood of forming cloud-free image pairs.

Apart from some scenarios and positions such as surges, spring speedups, and the margins of ice streams, glacier velocity gradients vary gradually in both space (low lateral velocity gradients) and time (low acceleration). Therefore, the accuracy of individual velocity measurements can be evaluated by comparing them to their immediate neighbours in both space and
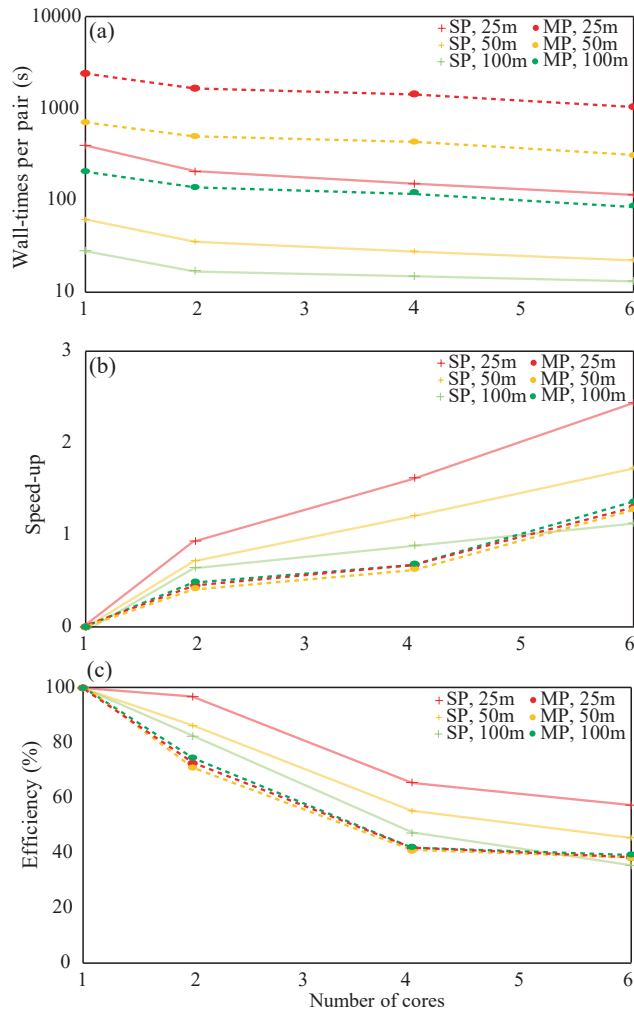
Figure 3. MP = Multi-pass; SP = Single-pass. Test conducted on a 12-image dataset of 10-m resolution, 1.7 million pixel images of Amalia Glacier, Chile using a Dell XPS 15 laptop ($2\times$16GB DDR4 2666 MHz memory, 6-core Intel i7-8750H 2.20 GHz processor). In all cases, parallelization decreases runtime, and going from one to two cores improves runtime by 1.4–1.9$\times$. Fine-resolution multi-pass runs usually yield the best velocity fields, and (b) shows that these benefit from the largest speed-up when parallelised.

time. Sudden jumps in space or time most likely represent erroneous velocities due to mismatches within the feature-tracking algorithm. This property is used in the GIV toolbox to improve the final velocity maps through the following workflow:

Firstly, GIV filters each individual velocity map through user-prescribed limits on velocity and flow direction, as well as outlier detection functions. This finds values that differ by more than 50% from their immediate neighbours (4 surrounding cells) and 200% from the mean of their larger local area (25 surrounding cells), removes these outlier values, and interpolates across these now-empty pixels using the remaining values. Secondly, GIV calculates the mean, standard deviation, median, minimum, and maximum velocities through time at each grid cell in the dataset. It then compares each individual value to

the mean value at that location for the entire dataset. Any values more than 1.5 standard deviations away from this mean are considered outliers. This process is carried out both for the velocity and flow-direction grids, and only values within the threshold for both velocity and flow direction are conserved. This provides an additional check, as erroneous values are unlikely to coincidentally match both the velocity and flow direction. Finally, the entire dataset may be smoothed and interpolated in space or time and space according to the user's choices. This allows missing values at one timestep to be linearly infilled from neighbouring times if the dataset is smooth enough to allow it. In addition, the displacement of each image pair may be normalized to the displacement of a user-defined stable ground mask to correct for systematic georeferencing errors.

Variable satellite repeat intervals and the exclusion of entirely clouded or otherwise unusable images lead to unevenly spaced velocity timeseries that are more difficult to interpret. In order to reduce this challenge, GIV includes a function that automatically averages the data and re-samples it to monthly intervals. This is easy when all individual velocity maps cover periods of less than one month and do not overlap between months, but becomes more complex when they do. In many cases, image pairs with the shortest lag times (<7–10 days) are excluded because displacement over such a short time may be obscured by offsets due to distortion and/or georeferencing errors. For the slowest-moving glaciers, this lower bound may be extended to several weeks or months. Lag times as long as the available imagery time series may be used so long as the surface of the glacier retains coherence in the image pairs.

GIV can determine monthly values by averaging across all image pairs that overlap with a given month. However, this produces an artificially smoothed dataset due to the influence of velocities measured across the boundaries of months. In order to make use of longer lag-time pairs, we develop an iterative strategy for calculating monthly values. In the first place, GIV takes a weighted mean of all velocities covering that month to make an initial guess at monthly velocities. The weighting parameter is determined by the proportion of the individual map contained within the given month, so for instance a velocity entirely within one month will be weighted 1 and one spread evenly over four months will be weighted 0.25. This initial estimate is then used to iterate between monthly averages and raw data values, with raw values covering more than one month split into monthly values by subtracting the previous iteration's estimate of monthly averages from them (Figure 4). This procedure may extract average monthly velocities even for months lacking any data. Outlier detection and maximum velocity filters are implemented to prevent small errors in the raw data from being accentuated by the iterations, but this may also lead to loss of data if too large a proportion of the initial dataset is inaccurate. Due to this limitation, the iterative calculations are not be adapted for some noisy datasets, in which the loss of temporal resolution by simple averaging will be preferable. Monthly averaging is performed as a post-processing step, and so may be repeated without the need to recalculate any raw velocity maps. Time series may also be generated from the raw data if monthly averaging is not desirable.

As a final step, GIV will automatically georeference the velocity grids and save .geotiff files to the user's computer. The toolbox also contains mapping tools that allow automatic generation of publication-quality images of the velocity and flow-direction maps (figure 5). Flow direction maps are plotted with a circular colormap, and all color maps used are color-blind friendly based on ?. In the following section we will examine some case studies of real glaciers and scenarios for which this model may be useful.
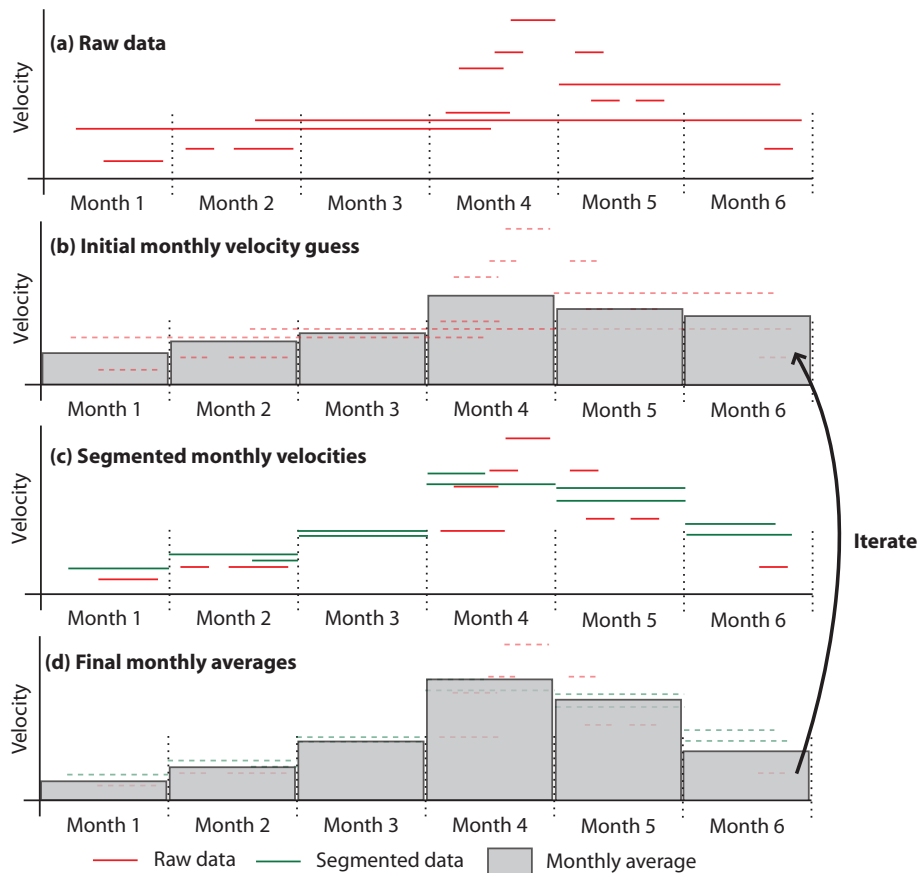
Figure 4. Schematic description of the techniques used to derive monthly velocities. The raw data (a) are combined in a weighted average to make an initial guess of monthly averages (b). The monthly averages are then used to segment longer time period velocity maps into their different monthly contributions (c). These are used to recalculate the monthly averages (d). Finally, GIV iterates over steps b–d for a number of times (e.g. 10) provided by user inputs. Note that an estimate may be made for the average velocity in 'Month 3', despite this month having no imagery available.

3   Results and Examples

Ice-velocity measurements supply essential information for studies of glacier dynamics, thickness, subglacial hydrology, and mass balance. With its GUI-based inputs and potential for parallelization, GIV can calculate a monthly velocity field for any glacier around the world with only a few hours of work. As such, it may also be run alongside field-based expeditions in order to understand the current conditions of the glacier and aid in instrumentation positioning.

We present four case studies. The first is of Glaciar Perito Moreno (50.48°S, 73.11°W), where we use GIV to determine the displacement of automated ablation stakes in conjunction with fieldwork in Spring 2020. The second is Glacier d'Argentiere (45.95°N, 06.97°E), a small and well-studied valley glacier located in the French Alps. The third is the Vavilov ice cap

(79.32°N, 94.34°E), located on October Revolution Island, in the Arctic Ocean off the mainland Russian coast, whose western outlet glacier is now surging into the ocean. Here we validate GIV against published results (Zheng et al., 2019b) using another image-based ice-velocity tool, CARST (Zheng et al., 2019a). Finally, we compute ice-flow velocities across the Chimborazo ice cap (01.45°S, 78.82°W) in Ecuador.

3.1 Field-campaign support: Glaciar Perito Moreno and the Southern Patagonian Icefield
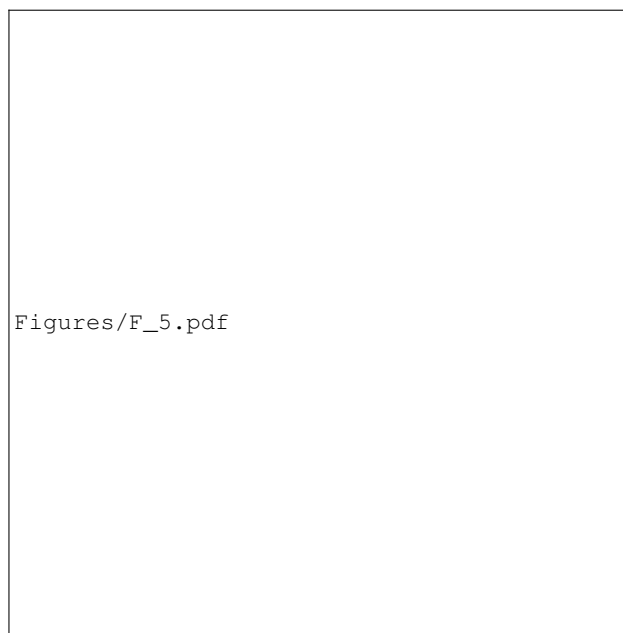
Figure 5. Mean flow velocity (m per year) (a) and direction (degrees) (b) of Glaciar Perito Moreno, Argentina for the first three months of 2020. Figure panels automatically generated from GIV, labels have been added and the color bars moved.

A team from the University of Minnesota installed 3 automated weather stations and 3 automated ablation stakes near the southern flank of Glaciar Perito Moreno in order to better understand the local conditions of this glacier and construct temperature-index and energy-balance models for glacier ablation. We installed the automated ablation stakes, based off of designs by Wickert (2014) and Wickert et al. (2019), and tested by Saberi et al. (2019) and Armstrong and Anderson (2020), for 20 days between the 23rd of February and 14th of March, 2020. In slowly flowing glaciers, ice flow may be largely neglected when considering equipment recovery. In rapidly flowing glaciers such as Perito Moreno, however, it may be relevant to consider the movement of the glacier when planning equipment recovery. This is particularly relevant where intense crevassing makes both access and visibility difficult. Figure 6 shows how different positioning decisions may influence ease of recovery: ablation stakes installed in position PM1 will move tens of metres towards the glacier calving front in less than a month, whereas stakes in position PM3 will move less than 5 m towards the glacier flank. In our survey, stakes were installed around position PM3 for ease of access.

Figure 6 (b) also presents the case of Glaciar Europa, which drains the adjacent portion of the Southern Patagonian Icefield in Chile. We also derived the mean velocity field of this glacier over the past 3 years using Sentinel-2 imagery (195 image pairs). GIV velocity measurements reveal that the central portion of Glaciar Europa at its outlet flows nearly 10,000 m/yr. If an ablation stake were installed in this area (point EU1), it would be displaced almost half a kilometre over the course of a 20-day survey. If it were instead placed at an alternative location 1 km to the West (EU2) it will be displaced only 20 metres in the same time period. This is an extreme case and the flow speeds of most glaciers are orders of magnitude slower, but showcases the potential value of deriving velocity fields for the success of a glaciological field campaign.
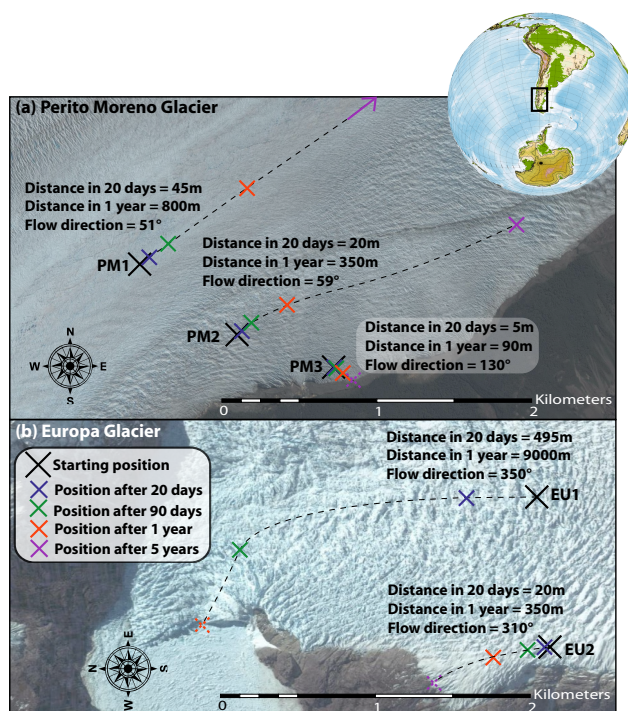
Figure 6. (a) Position of a point on Glaciar Perito Moreno with time for three different starting locations within 2 km of the glacier's southern margin. At PM1, ice speeds reach 800 m/yr and any equipment will be rapidly displaced. At PM3 ice-flow speeds are < 100 m per year and oriented towards the valley edge. (b) Identical plot for two points on Glaciar Europa. Any equipment installed at EU1 will be displaced several kilometres and lost to calving in less than 6 months. Imagery © Google Earth.

3.2 Valley-glacier velocity distribution: Glacier d'Argentière

In order to evaluate the effectiveness of GIV on smaller glaciers, we calculate a velocity field for a well-studied valley glacier in the Mont Blanc massif, Glacier d'Argentière (Benoit et al., 2015). We download one year worth of Sentinel-2 data (March 2019 – March 2020), containing over 1000 image pairs. These images are then used to derive a 25-m resolution mean-ice-velocity map, shown in Figure 7. The sparsity of features transverse to flow direction on Glacier d'Argentière make it difficult for

feature-tracking methods to calculate velocities. Nevertheless, the resulting flow-velocity map is comparable to those derived using a SPOT satellite image pair from 2003 (Berthier et al., 2005; Rabatel et al., 2018), SAR and ground based photogrammetry (Benoit et al., 2015), and a different feature-tracking routine based on a modified version of ampcor (Millan et al., 2019). The velocity map highlights accelerated ice flow at the terminus icefall and on the steep tributary glacier to the SW of the main trunk (Figure 7). Main-trunk velocities are on the order of 45–70 m/yr, slightly slower than Berthier et al. (2005)'s SPOT values but in line with Benoit et al. (2015)'s values. Our values represent the mean over an entire year, including the slower winter velocities captured by Berthier et al. (2005). It is also possible that glacier thinning has reduced its flow velocity, but our data is not sufficient to evaluate this.
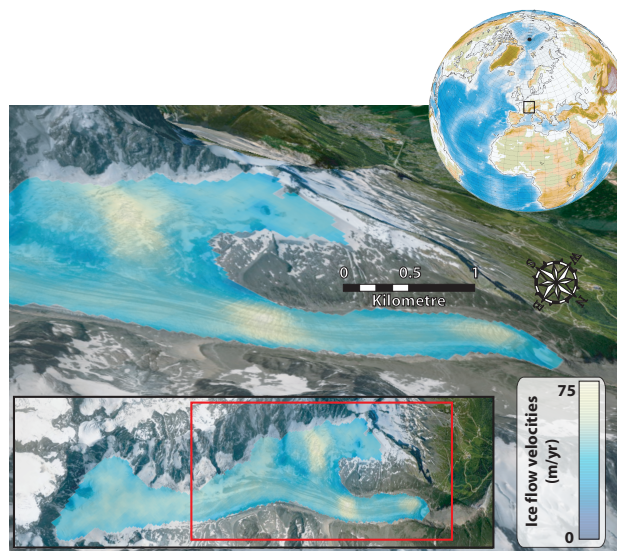
Figure 7. Perspective view of mean flow velocities of Glacier d'Argentière, France over the period 03/2019–03/2020. Imagery © Google Earth, scale for near margin of glacier.

3.3   Validating GIV by observing Vavilov ice cap dynamics

3.3.1   Mapping ice surge

Arctic land-ice melt has contributed more than 20 mm to global sea level rise since the 1970s (Box et al., 2018). Most of these large glaciers and ice caps remain remote and difficult to access, and high spatial and temporal resolution surface velocity maps provide one important tool to assess their response to changing environmental conditions.

Vavilov ice cap is a 1700 km^3 ice cap located on October Revolution Island in the Severnaya Zemlya archipelago, located in the Russian high arctic (Bassford et al., 2006). Until the 2010s, Vavilov ice cap exhibited surface velocities of only a few tens of metres per year, typical of many cold-based high-arctic ice masses. In 2013, a large portion of the marine-terminating western flank surged, with the ice front reaching more than 10 km beyond its prior grounding line by 2016 (Willis et al.,

2018; Zheng et al., 2019b). This sudden shift in ice behaviour was not accompanied by any dramatic climatic shift, and the exact triggers are a matter of active debate (Willis et al., 2018, and references therein). Willis et al. (2018) proposed that the dramatic acceleration is related to the ice cap overriding weak marine sediments in the Kara Sea, which can deform easily and substantially increase ice velocity. The ice cap margin is also no longer frozen to bedrock, leading to associated removal of resistive stresses at the ice front (Willis et al., 2018). Rapid ice flow initiates a set of internal feedbacks to further increase ice velocity, including strain softening of the ice itself; shear heating that produces meltwater, capable of reducing the effective normal stress of the ice and hence its friction against the bed; and potential infiltration of this water into the bed material, increasing its deformability (Willis et al., 2018, and references therein). With no direct data on subglacial conditions prior to or during the surge, the exact processes involved remain difficult to determine. We may, however, monitor surface ice velocities to examine the ongoing changes in ice kinematics.

Visible-band imagery from Vavilov ice cap is available only for summer months (March to September) due to darkness during the high-latitude boreal winter. We use GIV to derive a 100-m resolution ice-velocity map of a 365-km^2 area of the Western flank of the ice cap using the entire Sentinel-2 archive (beginning in 2016). Figure 8 (a) and (b) present two average yearly velocity maps for the apex of the surges in 2016 and 2019. Panels (d) and (e) present timeseries of monthly velocities over the period from March 2016 to March 2020 at the locations shown in figure 8(c).

Velocities of the centreline points converge over the time period considered: Although the velocities near the ice front decrease from the 2016 peak (red, orange, and green circles), velocities of regions most distant from the coast show a steady increase (purple points). The central portion of this newly formed outlet glacier shows distinct late-summer accelerations in both 2018 and 2019, reaching around double its spring and early summer rates and rapidly decaying (figure 7(d)). Within the newly formed western frontal lobe, extruded beyond the prior grounding line, flow has concentrated into a single branch with well-developed shear margins separating a central region with rapid ice flow from slow-moving lateral portions of the glacier (Zheng et al., 2019b).

Extraction of high-resolution ice velocities in this region using GIV confirms Willis et al. (2018) and Zheng et al. (2019b)'s findings that the western portion of Vavilov has entered into a new fast-flow regime. The late summer velocity peaks in both 2018 and 2019 may shed some light on the driving forces behind this acceleration if associated changed in climatic, ice surface or ice basal conditions are identified. Ongoing monitoring will help to determine whether a similar peak occurs in 2020 or any following years, and can be performed in near real time using GIV.

3.3.2 Method validation

We compare our GIV-derived results against a velocity map of the front of the western outlet glacier generated by Zheng et al. (2019b) using CARST (Zheng et al., 2019a). Zheng et al. (2019b) generated their velocity map based on a single Landsat 8 pair dated 2017/05/06 and 2017/05/22. We compared the ice-surface velocity magnitude calculated from this pair to the May 2017 average velocity map generated from Sentinel-2 imagery using GIV through the approach described above. We georeferenced the two velocity maps using the glacier margins and other notable features. The difference map (Fig. 9(a)) displays the highest amplitude anomalies along the margins of the central high-velocity band. Differences between the GIV- and CARST-derived
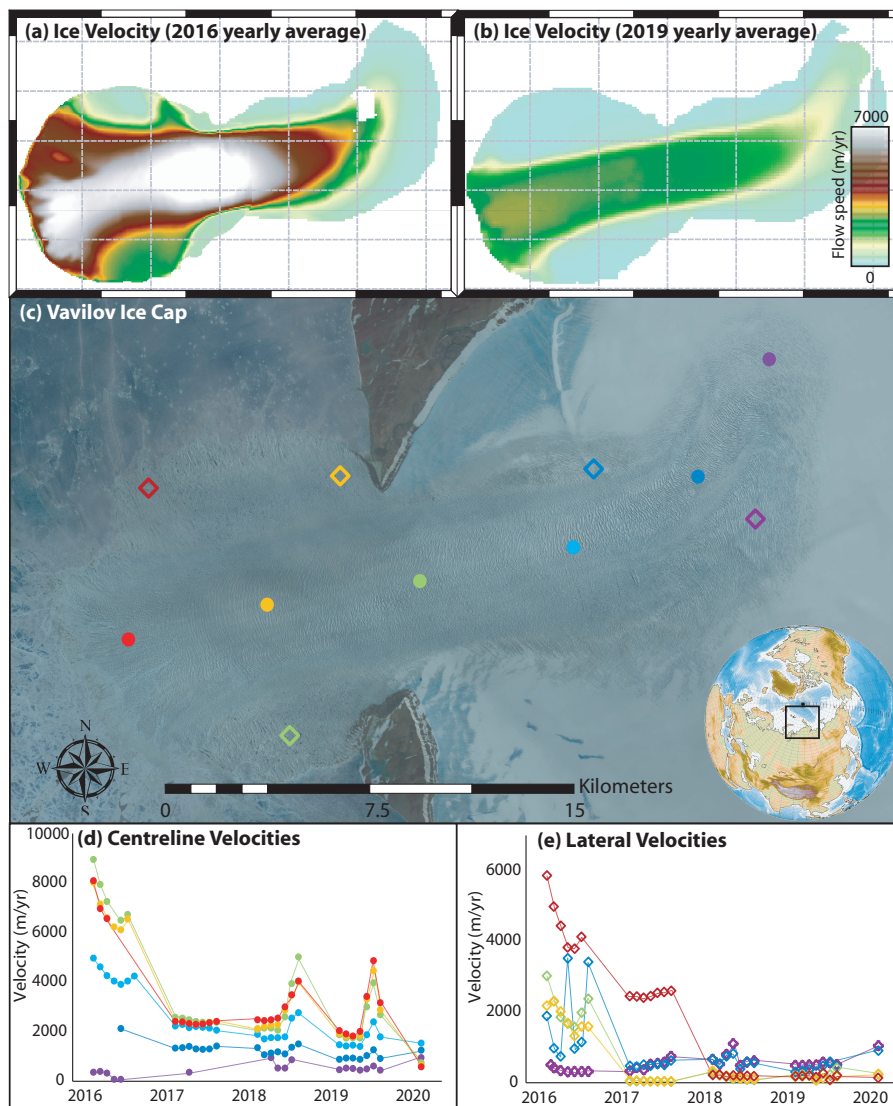
Figure 8. (a) and (b) present 100-m-resolution annual mean velocities for the western outlet glacier of Vavilov ice cap. (c) displays a 2019 Sentinel-2 image showing the main features of this outlet and the locations used to derive monthly timeseries. (d) and (e) present monthly resolution velocity timeseries along the glacier centreline and flanks using Sentinel-2 imagery.

velocity maps are normally distributed, with a mean difference of -16 m per year (Fig 9(c)). This mean difference is $\leq 1\%$ the speed across the majority of the glacier surface (Fig 9(b)). In this region of the glacier surface, the annual variability in ice-surface velocities is on the order of several hundred metres per year (Fig 8(d) and (e)), and this difference may result from the slightly different dates covered or differing image resolutions (10 m for Sentinel-2 compared to 15–30 m for Landsat).

The high-magnitude difference bands on either side of the fast-moving central region may also result in whole or part from georeferencing errors in GIV, in CARST, or in our work to georeference these two velocity maps to one another.
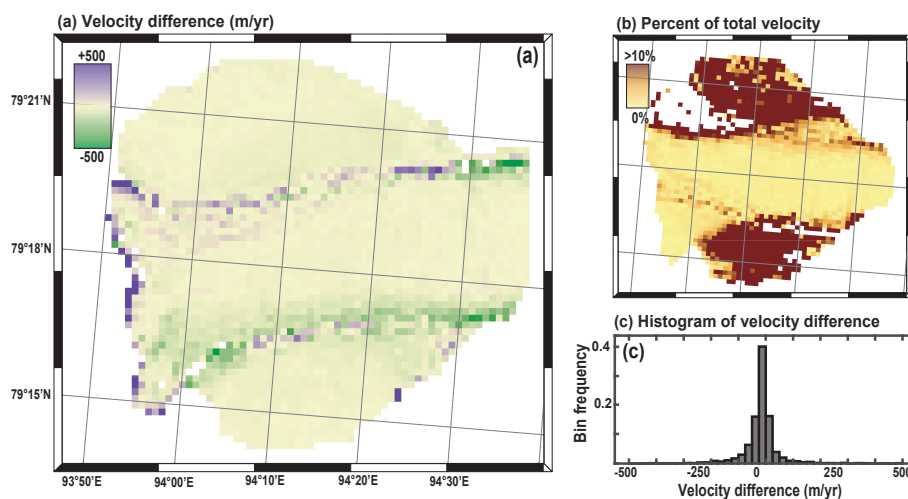
Figure 9. Comparison between Zheng et al. (2019b)'s velocity maps for Vavilov ice cap (Pair037_20170506_20170522) with results from GIV (May 2017 average). a) shows a difference map, corresponding to Zheng et al. velocity minus GIV velocity, b) shows what percentage of the total velocity this difference represents (absolute value of the difference shown in a) divided by GIV velocity), and c) is a histogram of the difference values. The mean difference between the two velocity maps is less than 20 m per year, or less than 1% of the total velocity for much of the area.

3.4 Ice-velocity of a small tropical ice cap: Chimborazo

Many tropical glaciers and ice caps have limited to no ice-flow data (Thompson et al., 2011). These are important water sources to millions of people (Bury et al., 2011; Chevallier et al., 2011; La Frenierre and Mark, 2017). Vergara et al. (2007) estimated the economic cost of glacier retreat on water use to be in the hundreds of millions of U.S. dollars, and the impact on Peru's electrical utility to be ~1.5 billion. High resolution estimates of ice velocity provide information on glacier state, and can contribute to practical decision making in the tropical Andes.

Chimborazo is a 6268 m high stratovolcano in Ecuador capped with an ice cap and 17 outlet glaciers. On Chimborazo's north-eastern flank, glacier meltwater drives nearly all of the discharge variability, and the disappearance of the prominent Reschreiter Glacier could decrease the discharge of the watershed's outlet stream by up to 50% (Saberi et al., 2019). Due to its high elevation and steep slopes that are unstable in regions of recent ice retreat, the glaciers on Chimborazo are difficult to survey (Saberi et al., 2019). No field measurements of glacier surface velocity have been conducted.

Chimborazo poses challenges to feature-tracking-based ice velocimetry, as its glaciers are small, regularly feature-poor or snow-covered, very slow moving, and cloud covered for large parts of the year. The velocity limitations are mitigated by using only images with large temporal separation (acquisition dates more than six months apart). GIV is also well suited for extracting

velocities from partially clouded imagery. We run GIV on the full Sentinel-2 dataset, which comprises of 91 individual partially or fully cloud-free images. These were cropped to Chimborazo, resulting in 3062 image pairs separated by at least six months. Resultant ice velocities for each pair were corrected for the mean displacement of a stable, non-glaciated region surrounding the ice cap. Results are shown in Figure 10. The runtime for this calculation is approximately 2 hours on a Dell XPS 15 laptop (2×16GB DDR4 2666 MHz memory, 6-core Intel i7-8750H 2.20 GHz processor).
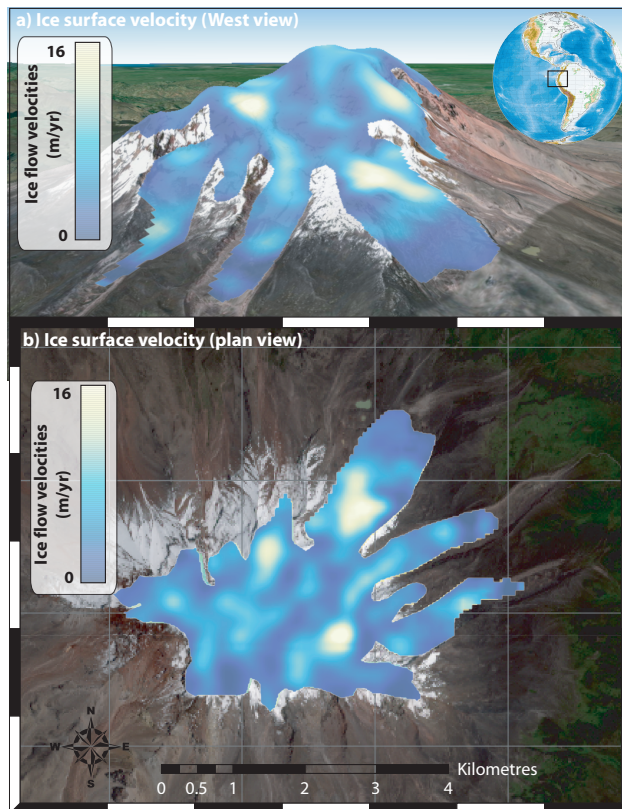
Figure 10. Ice-surface-velocity map for the Chimborazo ice cap calculated with GIV. Imagery © Google Earth and Sentinel-2.

4   Discussion

These four examples underline GIV's flexibility, ease of use, and ability to rapidly process large datasets for calculating ice velocities in a range of environments. Most regular laptop and desktop computers now include at least 4 cores, which GIV uses to speed up calculations by a factor of two or more (Figure 3). This makes velocity-field calculations with hundreds to thousands of image pairs practical on regular computers. The inclusion of 'temporal oversampling' allows much larger datasets to be generated than via simple consecutive-image comparison; a dataset of 100 images may in fact include several thousand usable image pairs. We combine methodological advances in feature tracking and image processing from both geoscience and

engineering toolboxes, and develop new filtering techniques to improve the quality of the final surface-velocity maps. GIV
340 provides a rapid and easy-to-use interface (shown in Figure 11) and a user manual, and may also be of use to communities who
would not generally be involved with glacier remote sensing (Van Wyk de Vries, 2020a, b).

Figure 11. Main graphical user interface for GIV, showing the main input fields. This interface may either be run through MATLAB or as an independent desktop app with no licensing requirements.

Many other feature-tracking algorithms have been used in glaciological research. These include CARST (Cryosphere and Remote Sensing Toolkit: Willis et al., 2018), COSI-corr (Co-registration of Optically Sensed Images and Correlation: Leprince et al., 2007b), AutoRIFT (Autonomous Repeat Image Feature Tracking: Gardner et al., 2018), ImGRAFT (Image Georectifi-
345 cation and Feature Tracking: Messerli and Grinsted, 2015), and SenDiT (the Sentinel-2 Displacement Toolbox: Nagy and Andreassen, 2019; Nagy et al., 2019). CARST contains a mixture of Python and Bash scripts used to monitor changes in glaciers,

and includes feature-tracking and ice-elevation-change-monitoring tools (Willis et al., 2018; Zheng et al., 2018, 2019a). COSI-Corr is a flexible co-registration and feature-tracking tool written in IDL, implemented in the ENVI GIS package, and initially used for measuring co-seismic deformation. Auto-RIFT is a Python-based feature-tracking algorithm (Gardner et al., 2018) with similar core components to GIV. It was used to calculate yearly resolution average velocity maps of the Antarctic and Greenland ice sheets (ITS_LIVE dataset). ImGRAFT is a MATLAB-based toolbox for georectifying and feature-tracking of ground based imagery, and may also be used on satellite imagery. SenDiT provides a platform to automatically download and generate velocity maps based on Sentinel-2 data, using a Python interface with bindings to the C- and Fortran-based *imcorr* toolbox (Scambos et al., 1992) for feature-tracking calculations.

In some circumstances, GIV will not be the most suitable feature tracking tool. For example, users who need to manually perform prior image co-registration (e.g. with airphotos) may wish to the built-in workflow in COSI-Corr. The objective of GIV is not to compete with or replace all the above tools, but rather to provide an easy-to-use, flexible, and robust alternative. GIV is easily learned and is not computationally time-consuming, and the results derived with it are easy to reproduce. GIV allows users to modify image-processing and feature-tracking parameters based on their expert knowledge of particular glaciers, without the need for specific computational knowledge. GIV may be run either directly through MATLAB functions, through a MATLAB graphical user interface (Van Wyk de Vries, 2020a), or as an independent desktop app that may be run with no MATLAB license (Van Wyk de Vries, 2020b). GIV has been tested and successfully run on Windows, Mac and Linux operating systems.

5 Conclusions

GIV is a versatile, GUI-based, and fully parallelised toolbox that enables rapid calculation of glacier velocity fields from satellite imagery. GIV ~~incorporates~~ builds upon recent improvements in optical satellite imagery availability and resolution to extract high temporal and spatial resolution velocity maps, and uses novel and pre-existing filters to optimise the quality of these velocity maps. GIV has been successfully tested on a wide range of environments, including small valley glaciers (Glacier d'Argentière, France), tropical ice caps (Volcán Chimborazo, Ecuador), and large outlet glaciers (Glaciar Perito Moreno, Argentina, and outflow from the Vavilov Ice Cap, Russia). We show that ice-velocity datasets are versatile and may be used to compliment field campaigns, and study the dynamics of large and small glaciers. Source code and pre-compiled binary executables for GIV are available from Van Wyk de Vries (2020a) and Van Wyk de Vries (2020b).

Code availability. MATLAB code for GIV may be downloaded from https://github.com/MaxVWDV/glacier-image-velocimetry (Van Wyk de Vries, 2020a). The GIV standalone app may be downloaded from https://github.com/MaxVWDV/glacier-image-velocimetry-app (Van Wyk de Vries, 2020b). Both include a user manual and examples.

Author contributions. MV and AW planned the project. MV wrote the code and ran the examples. MV and AW wrote and edited the manuscript.

Competing interests. The authors declare no competing interests.

Acknowledgements. MV was supported by a University of Minnesota College of Science and Engineering fellowship. Ben Popken assisted
380   with early testing of GIV. Emi Ito, Kelly MacGregor, Jeff La Frenierre, Matias Romero, Shanti B. Penprase, Jabari Jones and Kerry L. Callaghan provided comments on this manuscript. We thank Ted Scambos and ~~an~~ two anonymous reviewer for thoughtful reviews, which improved both the manuscript and associated toolbox. We further acknowledge editor Harry Zekollari for providing welcome feedback and suggestions. This material is based upon work supported by the National Science Foundation under Grant No. EAR-1714614, coordinated by Lead PI Maria Beatrice Magnani.

385 References

AghaKouchak, A., Farahmand, A., Melton, F. S., Teixeira, J., Anderson, M. C., Wardlow, B. D., and Hain, C. R.: Remote sensing of drought: Progress, challenges and opportunities, Reviews of Geophysics, 53, 452–480, https://doi.org/10.1002/2014RG000456, http://agupubs. onlinelibrary.wiley.com/doi/abs/10.1002/2014RG000456, _eprint: https://onlinelibrary.wiley.com/doi/pdf/10.1002/2014RG000456, 2015.

390 Altena, B.: Observing change in glacier flow by using optical satellites, https://www.duo.uio.no/handle/10852/61747, accepted: 2018-05-28T11:09:27Z, 2018.

Armstrong, W. H. and Anderson, R. S.: Ice-marginal lake hydrology and the seasonal dynamical evolution of Kennicott Glacier, Alaska, Journal of Glaciology, pp. 1–15, publisher: Cambridge University Press, 2020.

Bakke, J. and Nesje, A.: Equilibrium-Line Altitude (ELA), in: Encyclopedia of Snow, Ice and Glaciers, edited by Singh, V. P., Singh, P.,
395 and Haritashya, U. K., pp. 268–277, Springer Netherlands, Dordrecht, https://doi.org/10.1007/978-90-481-2642-2_140, https://doi.org/10. 1007/978-90-481-2642-2_140, 2011.

Bamber, J. L. and Rivera, A.: A review of remote sensing methods for glacier mass balance determination, Global and Planetary Change, 59, 138–148, https://doi.org/10.1016/j.gloplacha.2006.11.031, http://www.sciencedirect.com/science/article/pii/S0921818106003055, 2007.

Bassford, R. P., Siegert, M. J., Dowdeswell, J. A., Oerlemans, J., Glazovsky, A. F., and Macheret, Y. Y.: Quantifying the Mass
400 Balance of Ice Caps on Severnaya Zemlya, Russian High Arctic. I: Climate and Mass Balance of the Vavilov Ice Cap, Arctic, Antarctic, and Alpine Research, 38, 1–12, https://doi.org/10.1657/1523-0430(2006)038[0001:QTMBOI]2.0.CO;2, https://www. tandfonline.com/doi/abs/10.1657/1523-0430%282006%29038%5B0001%3AQTMBOI%5D2.0.CO%3B2, publisher: Taylor & Francis _eprint: https://www.tandfonline.com/doi/pdf/10.1657/1523-0430%282006%29038%5B0001%3AQTMBOI%5D2.0.CO%3B2, 2006.

Benoit, L., Dehecq, A., Pham, H.-T., Vernier, F., Trouvé, E., Moreau, L., Martin, O., Thom, C., Pierrot-Deseilligny, M., and Briole, P.: Multi-
405 method monitoring of Glacier d'Argentière dynamics, Annals of Glaciology, 56, 118–128, https://doi.org/10.3189/2015AoG70A985, https://www.cambridge.org/core/product/identifier/S0260305500250398/type/journal_article, 2015.

Berthier, E., Vadon, H., Baratoux, D., Arnaud, Y., Vincent, C., Feigl, K. L., Rémy, F., and Legrésy, B.: Surface motion of mountain glaciers derived from satellite optical imagery, Remote Sensing of Environment, 95, 14–28, https://doi.org/10.1016/j.rse.2004.11.005, http://www. sciencedirect.com/science/article/pii/S0034425704003463, 2005.

410 Bindschadler, R., Vornberger, P., Fleming, A., Fox, A., Mullins, J., Binnie, D., Paulsen, S. J., Granneman, B., and Gorodetzky, D.: The Landsat Image Mosaic of Antarctica, Remote Sensing of Environment, 112, 4214–4226, https://doi.org/10.1016/j.rse.2008.07.006, http: //www.sciencedirect.com/science/article/pii/S003442570800223X, 2008.

Bindschadler, R. A. and Scambos, T. A.: Satellite-Image-Derived Velocity Field of an Antarctic Ice Stream, Science, 252, 242–246, https://doi.org/10.1126/science.252.5003.242, https://science.sciencemag.org/content/252/5003/242, 1991.

415 Bottomley, J. T.: Flow of Viscous Materials—A Model Glacier, Nature, 21, 159–159, https://doi.org/10.1038/021159a0, http://www.nature. com/articles/021159a0, number: 529 Publisher: Nature Publishing Group, 1879.

Box, J. E., Colgan, W. T., Wouters, B., Burgess, D. O., O'Neel, S., Thomson, L. I., and Mernild, S. H.: Global sea-level contribution from Arctic land ice: 1971–2017, Environmental Research Letters, 13, 125 012, https://doi.org/10.1088/1748-9326/aaf2ed, https://doi.org/10. 1088%2F1748-9326%2Faaf2ed, publisher: IOP Publishing, 2018.

420 Buchhave, P.: Particle image velocimetry—status and trends, Experimental Thermal and Fluid Science, 5, 586–604, https://doi.org/10.1016/0894-1777(92)90016-X, http://www.sciencedirect.com/science/article/pii/089417779290016X, 1992.

Bury, J. T., Mark, B. G., McKenzie, J. M., French, A., Baraer, M., Huh, K. I., Zapata Luyo, M. A., and Gómez López, R. J.: Glacier recession and human vulnerability in the Yanamarey watershed of the Cordillera Blanca, Peru, Climatic Change, 105, 179–206, https://doi.org/10.1007/s10584-010-9870-1, https://doi.org/10.1007/s10584-010-9870-1, 2011.

425 Chadwell, C. D.: Reliability analysis for design of stake networks to measure glacier surface velocity, Journal of Glaciology, 45, 154–164, https://doi.org/10.3189/S0022143000003130, http://www.cambridge.org/core/journals/journal-of-glaciology/article/reliability-analysis-for-design-of-stake-networks-to-measure-glacier-surface-velocity/F342FD59DA4D2EA6689383D677351269, publisher: Cambridge University Press, 1999.

Chevallier, P., Pouyaud, B., Suarez, W., and Condom, T.: Climate change threats to environment in the tropical Andes: glaciers and water
430 resources, Regional Environmental Change, 11, 179–187, https://doi.org/10.1007/s10113-010-0177-6, http://link.springer.com/10.1007/s10113-010-0177-6, 2011.

Darji, S., Shah, R. D., Oza, S., and Bahuguna, I. M.: Inter-Comparison of Various Feature Tracking Tools Deriving Glacier Ice Velocity, 7, 8, 2018.

Davies, B. J. and Glasser, N. F.: Accelerating shrinkage of Patagonian glaciers from the Little Ice Age (~AD 1870) to 2011, Journal of Glaciol-
435 ogy, 58, 1063–1084, https://doi.org/10.3189/2012JoG12J026, https://www.cambridge.org/core/journals/journal-of-glaciology/article/accelerating-shrinkage-of-patagonian-glaciers-from-the-little-ice-age-ad-1870-to-2011/933AF3AB94615A1E7AACF85510FF7FD1, 2012.

Deeley, R. M. and Parr, P. H.: XVI. The Hintereis Glacier, The London, Edinburgh, and Dublin Philosophical Magazine and Journal of Science, 27, 153–176, publisher: Taylor & Francis, 1914.

440 Drusch, M., Del Bello, U., Carlier, S., Colin, O., Fernandez, V., Gascon, F., Hoersch, B., Isola, C., Laberinti, P., Martimort, P., Meygret, A., Spoto, F., Sy, O., Marchese, F., and Bargellini, P.: Sentinel-2: ESA's Optical High-Resolution Mission for GMES Operational Services, Remote Sensing of Environment, 120, 25–36, https://doi.org/10.1016/j.rse.2011.11.026, http://www.sciencedirect.com/science/article/pii/S0034425712000636, 2012.

Earl, L. and Gardner, A.: A satellite-derived glacier inventory for North Asia, Annals of Glaciology, 57, 50–
445 60, https://doi.org/10.3189/2016AoG71A008, http://www.cambridge.org/core/journals/annals-of-glaciology/article/satellitederived-glacier-inventory-for-north-asia/9CFCE79604C90AECCCAA5E0308D91B93, publisher: Cambridge University Press, 2016.

Fahnestock, M., Scambos, T., Moon, T., Gardner, A., Haran, T., and Klinger, M.: Rapid large-area mapping of ice flow using Landsat 8, Remote Sensing of Environment, 185, 84–94, https://doi.org/10.1016/j.rse.2015.11.023, http://www.sciencedirect.com/science/article/pii/
450 S003442571530211X, 2016.

Fitch, A., Kadyrov, A., Christmas, W., and Kittler, J.: Orientation Correlation, in: Procedings of the British Machine Vision Conference 2002, pp. 11.1–11.10, British Machine Vision Association, Cardiff, https://doi.org/10.5244/C.16.11, http://www.bmva.org/bmvc/2002/papers/95/index.html, 2002.

Forbes, J. D.: The Glacier Theory, google-Books-ID: wPoTAAAAQAAJ, 1840.

455 Forbes, J. D.: XII. Illustrations of the viscous theory of glacier motion. - Part I. Containing experiments on the flow of plastic bodies, and observations on the phenomena of lava streams, Philosophical Transactions of the Royal Society of London, 136, 143–155, https://doi.org/10.1098/rstl.1846.0013, https://royalsocietypublishing.org/doi/abs/10.1098/rstl.1846.0013, publisher: Royal Society, 1846.

Fowler, A.: Weertman, Lliboutry and the development of sliding theory, Journal of Glaciology, 56, 965–972, https://doi.org/10.3189/002214311796406112, https://www.cambridge.org/core/product/identifier/S0022143000213191/type/journal_article, 2010.

Frigo, M. and Johnson, S.: FFTW: an adaptive software architecture for the FFT, in: Proceedings of the 1998 IEEE International Conference on Acoustics, Speech and Signal Processing, ICASSP '98 (Cat. No.98CH36181), vol. 3, pp. 1381–1384, IEEE, Seattle, WA, USA, https://doi.org/10.1109/ICASSP.1998.681704, http://ieeexplore.ieee.org/document/681704/, 1998.

Frigo, M. and Johnson, S.: The Design and Implementation of FFTW3, Proceedings of the IEEE, 93, 216–231, https://doi.org/10.1109/JPROC.2004.840301, conference Name: Proceedings of the IEEE, 2005.

Gardner, A., Fahnestock, M., and Scambos, T.: ITS_LIVE Regional Glacier and Ice Sheet Surface Velocities., doi:10.5067/6II6VW8LLWJ7, 2020.

Gardner, A. S., Moholdt, G., Scambos, T., Fahnstock, M., Ligtenberg, S., Broeke, M. v. d., and Nilsson, J.: Increased West Antarctic and unchanged East Antarctic ice discharge over the last 7 years, The Cryosphere, 12, 521–547, https://doi.org/https://doi.org/10.5194/tc-12-521-2018, https://www.the-cryosphere.net/12/521/2018/, publisher: Copernicus GmbH, 2018.

Grant, I.: Particle image velocimetry: A review, Proceedings of the Institution of Mechanical Engineers, Part C: Journal of Mechanical Engineering Science, 211, 55–76, https://doi.org/10.1243/0954406971521665, https://doi.org/10.1243/0954406971521665, publisher: IMECHE, 1997.

Harris, A.: Thermal Remote Sensing of Active Volcanoes: A User's Manual, Cambridge University Press, google-Books-ID: xY4oYzbH0ooC, 2013.

Heid, T. and Kääb, A.: Evaluation of existing image matching methods for deriving glacier surface displacements globally from optical satellite imagery, Remote Sensing of Environment, 118, 339–355, https://doi.org/10.1016/j.rse.2011.11.024, http://www.sciencedirect.com/science/article/pii/S0034425711004214, 2012a.

Heid, T. and Kääb, A.: Repeat optical satellite images reveal widespread and long term decrease in land-terminating glacier speeds, The Cryosphere, 6, 467–478, https://doi.org/10.5194/tc-6-467-2012, https://www.the-cryosphere.net/6/467/2012/, 2012b.

Hooke, R. L., Calla, P., Holmlund, P., Nilsson, M., and Stroeven, A.: A 3 Year Record of Seasonal Variations in Surface Velocity, StorglaciÄren, Sweden, Journal of Glaciology, 35, 235–247, https://doi.org/10.3189/S0022143000004561, http://www.cambridge.org/core/journals/journal-of-glaciology/article/3-year-record-of-seasonal-variations-in-surface-velocity-storglaciaren-sweden/2BF67175ACC7E8843B2AC980C4804F4A, publisher: Cambridge University Press, 1989.

How, P., Hulton, N. R. J., Buie, L., and Benn, D. I.: PyTrx: A Python-Based Monoscopic Terrestrial Photogrammetry Toolset for Glaciology, Frontiers in Earth Science, 8, https://doi.org/10.3389/feart.2020.00021, https://www.frontiersin.org/articles/10.3389/feart.2020.00021/full, publisher: Frontiers, 2020.

Howat, I. M., Negrete, A., and Smith, B.: The Greenland Ice Mapping Project (GIMP) land classification and surface elevation data sets, https://doi.org/10.5194/tc-8-1509-2014, 2014.

Howat, I. M., Porter, C., Smith, B. E., Noh, M.-J., and Morin, P.: The Reference Elevation Model of Antarctica, The Cryosphere, 13, 665–674, https://doi.org/https://doi.org/10.5194/tc-13-665-2019, https://tc.copernicus.org/articles/13/665/2019/, publisher: Copernicus GmbH, 2019.

Hui, F., Cheng, X., Liu, Y., Zhang, Y., Ye, Y., Wang, X., Li, Z., Wang, K., Zhan, Z., Guo, J., Huang, H., Li, X., Guo, Z., and Gong, P.: An improved Landsat Image Mosaic of Antarctica, Science China Earth Sciences, 56, 1–12, https://doi.org/10.1007/s11430-012-4481-5, https://doi.org/10.1007/s11430-012-4481-5, 2013.

James, M. R., How, P., and Wynn, P. M.: Pointcatcher software: analysis of glacial time-lapse photography and integration with multitemporal digital elevation models, Journal of Glaciology, 62, 159–169, https://doi.org/10.1017/jog.2016.27, http://www.cambridge.org/core/journals/journal-of-glaciology/article/pointcatcher-software-analysis-of-glacial-timelapse-photography-and-integration-with-multitemporal-digital-elevation-models/23EC92804DE7C5EED7229D0ACE31D90B, publisher: Cambridge University Press, 2016.

Jawak, S. D., Kumar, S., Luis, A. J., Bartanwala, M., Tummala, S., and Pandey, A. C.: Evaluation of Geospatial Tools for Generating Accurate Glacier Velocity Maps from Optical Remote Sensing Data, Proceedings, 2, 341, https://doi.org/10.3390/ecrs-2-05154, https://www.mdpi.com/2504-3900/2/7/341, 2018.

Kamb, B. and LaChapelle, E.: Direct Observation of the Mechanism of Glacier Sliding Over Bedrock*, Journal of Glaciology, 5, 159–172, https://doi.org/10.3189/S0022143000028756, http://www.cambridge.org/core/journals/journal-of-glaciology/article/direct-observation-of-the-mechanism-of-glacier-sliding-over-bedrock/A032752BFEA9BB2628AC95966D72C332, publisher: Cambridge University Press, 1964.

Klemas, V. V.: The Role of Remote Sensing in Predicting and Determining Coastal Storm Impacts, Journal of Coastal Research, 25, 1264–1275, https://doi.org/10.2112/08-1146.1, https://meridian.allenpress.com/jcr/article/25/6(256)/1264/28316/The-Role-of-Remote-Sensing-in-Predicting-and, publisher: Allen Press, 2009.

Kobayashi, T. and Otsu, N.: Image Feature Extraction Using Gradient Local Auto-Correlations, Computer Vision - ECCV 2008, 10th European Conference on Computer Vision, 2008.

Kääb, A. and Vollmer, M.: Surface Geometry, Thickness Changes and Flow Fields on Creeping Mountain Permafrost: Automatic Extraction by Digital Image Analysis, Permafrost and Periglacial Processes, 11, 315–326, https://doi.org/10.1002/1099-1530(200012)11:4<315::AID-PPP365>3.0.CO;2-J, http://onlinelibrary.wiley.com/doi/abs/10.1002/1099-1530%28200012%2911%3A4%3C315%3A%3AAID-PPP365%3E3.0.CO%3B2-J, _eprint: https://onlinelibrary.wiley.com/doi/pdf/10.1002/1099-1530%28200012%2911%3A4%3C315%3A%3AAID-PPP365%3E3.0.CO%3B2-J, 2000.

Kääb, A., Winsvold, S. H., Altena, B., Nuth, C., Nagler, T., and Wuite, J.: Glacier Remote Sensing Using Sentinel-2. Part I: Radiometric and Geometric Performance, and Application to Ice Velocity, Remote Sensing, 8, 598, https://doi.org/10.3390/rs8070598, https://www.mdpi.com/2072-4292/8/7/598, number: 7 Publisher: Multidisciplinary Digital Publishing Institute, 2016.

La Frenierre, J. and Mark, B. G.: Detecting Patterns of Climate Change at Volcán Chimborazo, Ecuador, by Integrating Instrumental Data, Public Observations, and Glacier Change Analysis, Annals of the American Association of Geographers, 107, 979–997, https://doi.org/10.1080/24694452.2016.1270185, https://doi.org/10.1080/24694452.2016.1270185, publisher: Taylor & Francis _eprint: https://doi.org/10.1080/24694452.2016.1270185, 2017.

Lee, R. M., Yue, H., Rappel, W.-J., and Losert, W.: Data from: Inferring single cell behavior from large-scale epithelial sheet migration patterns, https://doi.org/https://doi.org/10.13016/M2855R, http://drum.lib.umd.edu/handle/1903/19190, accepted: 2017-04-12T17:46:08Z type: dataset, 2017.

Leprince, S., Ayoub, F., Klinger, Y., and Avouac, J.-P.: Co-Registration of Optically Sensed Images and Correlation (COSI-Corr): an operational methodology for ground deformation measurements, in: 2007 IEEE International Geoscience and Remote Sensing Symposium, pp. 1943–1946, IEEE, Barcelona, Spain, https://doi.org/10.1109/IGARSS.2007.4423207, http://ieeexplore.ieee.org/document/4423207/, 2007a.

Leprince, S., Barbot, S., Ayoub, F., and Avouac, J.-P.: Automatic and Precise Orthorectification, Coregistration, and Subpixel Correlation of Satellite Images, Application to Ground Deformation Measurements, IEEE Transactions on Geoscience and Remote Sensing, 45, 1529–1558, https://doi.org/10.1109/TGRS.2006.888937, 2007b.

535 Mair, D., Willis, I., Fischer, U. H., Hubbard, B., Nienow, P., and Hubbard, A.: Hydrological controls on patterns of surface, internal and basal motion during three "spring events": Haut Glacier d'Arolla, Switzerland, Journal of Glaciology, 49, 555–567, https://doi.org/10.3189/172756503781830467, http://www.cambridge.org/core/journals/journal-of-glaciology/article/hydrological-controls-on-patterns-of-surface-internal-and-basal-motion-during-three-spring-events-haut-glacier-darolla-switzerland/9C10F4D8C42938F396AEF8E372F55247, publisher: Cambridge University Press, 2003.

540 Marc, O. and Hovius, N.: Amalgamation in landslide maps: effects and automatic detection, Natural Hazards and Earth System Sciences, 15, 723–733, https://doi.org/https://doi.org/10.5194/nhess-15-723-2015, https://www.nat-hazards-earth-syst-sci.net/15/723/2015/nhess-15-723-2015.html, publisher: Copernicus GmbH, 2015.

Meier, M. F. and Tangborn, W. V.: Net Budget and Flow of South Cascade Glacier, Washington, Journal of Glaciology, 5, 547–566, https://doi.org/10.3189/S0022143000018608, http://www.cambridge.org/core/journals/journal-of-glaciology/article/

545 net-budget-and-flow-of-south-cascade-glacier-washington/440E67FA2A6041F58689DDBB65733502, publisher: Cambridge University Press, 1965.

Messerli, A. and Grinsted, A.: Image georectification and feature tracking toolbox: ImGRAFT, Geoscientific Instrumentation, Methods and Data Systems, 4, 23–34, https://doi.org/10.5194/gi-4-23-2015, https://www.geosci-instrum-method-data-syst.net/4/23/2015/, 2015.

Metternicht, G., Hurni, L., and Gogu, R.: Remote sensing of landslides: An analysis of the potential contribution to

550 geo-spatial systems for hazard assessment in mountainous environments, Remote Sensing of Environment, 98, 284–303, https://doi.org/10.1016/j.rse.2005.08.004, http://www.sciencedirect.com/science/article/pii/S0034425705002506, 2005.

Millan, R.: Ice thickness and bed elevation of the Patagonian Icefields, https://doi.org/10.7280/d11q17, https://dash.lib.uci.edu/stash/dataset/doi:10.7280/D11Q17, type: dataset, 2019.

Millan, R., Mouginot, J., Rabatel, A., Jeong, S., Cusicanqui, D., Derkacheva, A., and Chekki, M.: Mapping Surface Flow Velocity of

555 Glaciers at Regional Scale Using a Multiple Sensors Approach, Remote Sensing, 11, 2498, https://doi.org/10.3390/rs11212498, https://www.mdpi.com/2072-4292/11/21/2498, number: 21 Publisher: Multidisciplinary Digital Publishing Institute, 2019.

Minchew, B. M., Simons, M., Riel, B., and Milillo, P.: Tidally induced variations in vertical and horizontal motion on Rutford Ice Stream, West Antarctica, inferred from remotely sensed observations, Journal of Geophysical Research: Earth Surface, 122, 167–190, https://doi.org/10.1002/2016JF003971, http://agupubs.onlinelibrary.wiley.com/doi/abs/10.1002/2016JF003971, _eprint:

560 https://onlinelibrary.wiley.com/doi/pdf/10.1002/2016JF003971, 2017.

Mote, T. L.: Greenland surface melt trends 1973–2007: Evidence of a large increase in 2007, Geophysical Research Letters, 34, https://doi.org/10.1029/2007GL031976, http://agupubs.onlinelibrary.wiley.com/doi/abs/10.1029/2007GL031976, _eprint: https://onlinelibrary.wiley.com/doi/pdf/10.1029/2007GL031976, 2007.

Mouginot, J. and Rignot, E.: Ice motion of the Patagonian Icefields of South America: 1984–2014, Geophysical Research Letters, 42, 1441–

565 1449, https://doi.org/10.1002/2014GL062661, https://agupubs.onlinelibrary.wiley.com/doi/full/10.1002/2014GL062661, 2015.

Nagy, T. and Andreassen, L. M.: Glacier surface velocity mapping with Sentinel-2 imagery in Norway, 2019.

Nagy, T., Andreassen, L. M., Duller, R. A., and Gonzalez, P. J.: SenDiT: The Sentinel-2 Displacement Toolbox with Application to Glacier Surface Velocities, Remote Sensing, 11, 1151, https://doi.org/10.3390/rs11101151, https://www.mdpi.com/2072-4292/11/10/1151, number: 10 Publisher: Multidisciplinary Digital Publishing Institute, 2019.

570   Nye, J. F.: The Mechanics of Glacier Flow, Journal of Glaciology, 2, 82–93, https://doi.org/10.3189/S0022143000033967, http://www.cambridge.org/core/journals/journal-of-glaciology/article/mechanics-of-glacier-flow/5FB3C31120796459A837491ACB085F32, publisher: Cambridge University Press, 1952.

Nye, J. F.: Glacier sliding without cavitation in a linear viscous approximation, Proceedings of the Royal Society of London. A. Mathematical and Physical Sciences, 315, 381–403, publisher: The Royal Society London, 1970.

575   Oertel, M. and Süfke, F.: Two-dimensional dam-break wave analysis: particle image velocimetry versus optical flow, Journal of Hydraulic Research, 58, 326–334, https://doi.org/10.1080/00221686.2019.1579114, https://doi.org/10.1080/00221686.2019.1579114, publisher: Taylor & Francis _eprint: https://doi.org/10.1080/00221686.2019.1579114, 2020.

Pfeffer, W. T., Arendt, A. A., Bliss, A., Bolch, T., Cogley, J. G., Gardner, A. S., Hagen, J.-O., Hock, R., Kaser, G., Kienholz, C., Miles, E. S., Moholdt, G., Mölg, N., Paul, F., Radić, V., Rastner, P., Raup, B. H., Rich, J., Sharp, M. J., and Consortium, T. R.: The Randolph Glacier
580   Inventory: a globally complete inventory of glaciers, Journal of Glaciology, 60, 537–552, https://doi.org/10.3189/2014JoG13J176, http://www.cambridge.org/core/journals/journal-of-glaciology/article/randolph-glacier-inventory-a-globally-complete-inventory-of-glaciers/730D4CC76E0E3EC1832FA3F4D90691CE, publisher: Cambridge University Press, 2014.

Porter, C., Morin, P., Howat, I., Noh, M.-J., Bates, B., Peterman, K., Keesey, S., Schlenk, M., Gardiner, J., Tomko, K., Willis, M., Kelleher, C., Cloutier, M., Husby, E., Foga, S., Nakamura, H., Platson, M., Wethington, M., Williamson, C., Bauer, G., Enos, J., Arnold, G., Kramer,
585   W., Becker, P., Doshi, A., D'Souza, C., Cummens, P., Laurier, F., and Bojesen, M.: ArcticDEM, https://doi.org/10.7910/DVN/OHHUKH, https://dataverse.harvard.edu/dataset.xhtml?persistentId=doi:10.7910/DVN/OHHUKH, publisher: Harvard Dataverse type: dataset, 2018.

Rabatel, A., Dedieu, J.-P., Thibert, E., Letréguilly, A., and Vincent, C.: 25 years (1981–2005) of equilibrium-line altitude and mass-balance reconstruction on Glacier Blanc, French Alps, using remote-sensing methods and meteorological data, Journal of Glaciology, 54, 307–314, https://doi.org/10.3189/002214308784886063, http://www.cambridge.org/core/journals/journal-of-glaciology/article/
590   25-years-19812005-of-equilibriumline-altitude-and-massbalance-reconstruction-on-glacier-blanc-french-alps-using-remotesensing-methods-and-me DB04ED9DE41C79FCA126917511C8A08E, publisher: Cambridge University Press, 2008.

Rabatel, A., Sanchez, O., Vincent, C., and Six, D.: Estimation of Glacier Thickness From Surface Mass Balance and Ice Flow Velocities: A Case Study on Argentière Glacier, France, Frontiers in Earth Science, 6, https://doi.org/10.3389/feart.2018.00112, https://www.frontiersin.org/articles/10.3389/feart.2018.00112/full, publisher: Frontiers, 2018.

595   Raffel, M., Willert, C. E., Scarano, F., Kähler, C. J., Wereley, S. T., and Kompenhans, J.: Particle Image Velocimetry: A Practical Guide, Springer, google-Books-ID: wk9UDwAAQBAJ, 2018.

Rhee, J., Im, J., and Carbone, G. J.: Monitoring agricultural drought for arid and humid regions using multi-sensor remote sensing data, Remote Sensing of Environment, 114, 2875–2887, https://doi.org/10.1016/j.rse.2010.07.005, http://www.sciencedirect.com/science/article/pii/S003442571000221X, 2010.

600   Rignot, E., Mouginot, J., and Scheuchl, B.: Ice Flow of the Antarctic Ice Sheet, Science, 333, 1427–1430, https://doi.org/10.1126/science.1208336, https://science.sciencemag.org/content/333/6048/1427, publisher: American Association for the Advancement of Science Section: Report, 2011.

Saberi, L., McLaughlin, R. T., Ng, G.-H. C., Frenierre, J. L., Wickert, A. D., Baraer, M., Zhi, W., Li, L., and Mark, B. G.: Multi-scale temporal variability in meltwater contributions in a tropical glacierized watershed, Hydrology and Earth System
605   Sciences, 23, 405–425, https://doi.org/https://doi.org/10.5194/hess-23-405-2019, https://www.hydrol-earth-syst-sci.net/23/405/2019/hess-23-405-2019.html, publisher: Copernicus GmbH, 2019.

Scambos, M. F. T.: Global Land Ice Velocity Extraction from Landsat 8 (GoLIVE), https://doi.org/10.7265/N5ZP442B, https://nsidc.org/data/nsidc-0710, type: dataset, 2016.

Scambos, T. A., Dutkiewicz, M. J., Wilson, J. C., and Bindschadler, R. A.: Application of image cross-correlation to the measurement of glacier velocity using satellite image data, Remote Sensing of Environment, 42, 177–186, https://doi.org/10.1016/0034-4257(92)90101-O, http://www.sciencedirect.com/science/article/pii/003442579290101O, 1992.

Scambos, T. A., Haran, T. M., Fahnestock, M. A., Painter, T. H., and Bohlander, J.: MODIS-based Mosaic of Antarctica (MOA) data sets: Continent-wide surface morphology and snow grain size, Remote Sensing of Environment, 111, 242–257, https://doi.org/10.1016/j.rse.2006.12.020, http://www.sciencedirect.com/science/article/pii/S0034425707002854, 2007.

Schwalbe, E. and Maas, H.-G.: The determination of high-resolution spatio-temporal glacier motion fields from time-lapse sequences, Earth Surface Dynamics, 5, 861–879, https://doi.org/10.5194/esurf-5-861-2017, https://www.earth-surf-dynam.net/5/861/2017/, 2017.

Shean, D.: dshean/vmap: Zenodo DOI release, https://doi.org/10.5281/zenodo.3243479, https://zenodo.org/record/3243479#.XwiOvihKhPY, 2019.

Sneed, W. A. and Hamilton, G. S.: Evolution of melt pond volume on the surface of the Greenland Ice Sheet, Geophysical Research Letters, 34, https://doi.org/10.1029/2006GL028697, http://agupubs.onlinelibrary.wiley.com/doi/abs/10.1029/2006GL028697, _eprint: https://onlinelibrary.wiley.com/doi/pdf/10.1029/2006GL028697, 2007.

Stearns, L. A., Smith, B. E., and Hamilton, G. S.: Increased flow speed on a large East Antarctic outlet glacier caused by subglacial floods, Nature Geoscience, 1, 827–831, https://doi.org/10.1038/ngeo356, http://www.nature.com/articles/ngeo356, number: 12 Publisher: Nature Publishing Group, 2008.

Stocker, T. F., Qin, D., Plattner, G.-K., Tignor, M., Allen, S. K., Boschung, J., Nauels, A., Xia, Y., Bex, V., and Midgley, P. M.: Climate change 2013: The physical science basis, Contribution of working group I to the fifth assessment report of the intergovernmental panel on climate change, 1535, publisher: Cambridge university press Cambridge, United Kingdom and New York, NY, USA, 2013.

Sveen, J. K.: An introduction to MatPIV v. 1.6.1, https://www.duo.uio.no/handle/10852/10196, accepted: 2013-03-12T08:18:23Z Publisher: Matematisk Institutt, Universitetet i Oslo, 2004.

Sveen, J. K. and Cowen, E. A.: Quantitative imaging techniques and their application to wavy flows, in: PIV and Water Waves, vol. Volume 9 of *Advances in Coastal and Ocean Engineering*, pp. 1–49, WORLD SCIENTIFIC, https://doi.org/10.1142/9789812796615_0001, https://www.worldscientific.com/doi/abs/10.1142/9789812796615_0001, 2004.

Thielicke, W. and Stamhuis, E.: PIVlab – Towards User-friendly, Affordable and Accurate Digital Particle Image Velocimetry in MATLAB, Journal of Open Research Software, 2, e30, https://doi.org/10.5334/jors.bl, http://openresearchsoftware.metajnl.com/articles/10.5334/jors.bl/, number: 1 Publisher: Ubiquity Press, 2014.

Thompson, L. G., Mosley-Thompson, E., Davis, M. E., and Brecher, H. H.: Tropical glaciers, recorders and indicators of climate change, are disappearing globally, Annals of Glaciology, 52, 23–34, https://doi.org/10.3189/172756411799096231, https://www.cambridge.org/core/product/identifier/S0260305500250957/type/journal_article, 2011.

Tralli, D. M., Blom, R. G., Zlotnicki, V., Donnellan, A., and Evans, D. L.: Satellite remote sensing of earthquake, volcano, flood, landslide and coastal inundation hazards, ISPRS Journal of Photogrammetry and Remote Sensing, 59, 185–198, https://doi.org/10.1016/j.isprsjprs.2005.02.002, http://www.sciencedirect.com/science/article/pii/S0924271605000043, 2005.

Van Wyk de Vries, M.: Glacier Image Velocimetry (GIV), https://doi.org/10.5281/zenodo.4159875, https://zenodo.org/record/4144839#.X5l7OtD7RPY, 2020a.

Van Wyk de Vries, M.: Glacier Image Velocimetry (GIV) app, https://doi.org/10.5281/zenodo.4147589, https://zenodo.org/record/4144854#
.X5l7Z9D7RPY, 2020b.

Vergara, W., Deeb, A., Valencia, A., Bradley, R., Francou, B., Zarzar, A., Grünwaldt, A., and Haeussling, S.: Eco-
nomic impacts of rapid glacier retreat in the Andes, Eos, Transactions American Geophysical Union, 88, 261–264,
https://doi.org/10.1029/2007EO250001, http://agupubs.onlinelibrary.wiley.com/doi/abs/10.1029/2007EO250001, _eprint:
https://onlinelibrary.wiley.com/doi/pdf/10.1029/2007EO250001, 2007.

Wal, R. S. W. v. d., Boot, W., Broeke, M. R. v. d., Smeets, C. J. P. P., Reijmer, C. H., Donker, J. J. A., and Oerlemans,
J.: Large and Rapid Melt-Induced Velocity Changes in the Ablation Zone of the Greenland Ice Sheet, Science, 321, 111–113,
https://doi.org/10.1126/science.1158540, https://science.sciencemag.org/content/321/5885/111, publisher: American Association for the
Advancement of Science Section: Report, 2008.

Weertman, J.: On the Sliding of Glaciers, Journal of Glaciology, 3, 33–38, https://doi.org/10.3189/S0022143000024709, http://www.
cambridge.org/core/journals/journal-of-glaciology/article/on-the-sliding-of-glaciers/E16342853EE9ED61ED1CDE79FE3BF4C5, pub-
lisher: Cambridge University Press, 1957.

Wickert, A. D.: The ALog: Inexpensive, Open-Source, Automated Data Collection in the Field, The Bulletin of the Ecological So-
ciety of America, 95, 166–176, https://doi.org/10.1890/0012-9623-95.2.68, https://esajournals.onlinelibrary.wiley.com/doi/abs/10.1890/
0012-9623-95.2.68, _eprint: https://esajournals.onlinelibrary.wiley.com/doi/pdf/10.1890/0012-9623-95.2.68, 2014.

Wickert, A. D., Sandell, C. T., Schulz, B., and Ng, G.-H. C.: Open-source Arduino-compatible data loggers designed for field re-
search, Hydrology and Earth System Sciences, 23, 2065–2076, https://doi.org/https://doi.org/10.5194/hess-23-2065-2019, https://www.
hydrol-earth-syst-sci.net/23/2065/2019/, publisher: Copernicus GmbH, 2019.

Willis, M. J., Zheng, W., Durkin, W. J., Pritchard, M. E., Ramage, J. M., Dowdeswell, J. A., Benham, T. J., Bassford, R. P., Stearns, L. A.,
Glazovsky, A. F., Macheret, Y. Y., and Porter, C. C.: Massive destabilization of an Arctic ice cap, Earth and Planetary Science Letters,
502, 146–155, https://doi.org/10.1016/j.epsl.2018.08.049, http://www.sciencedirect.com/science/article/pii/S0012821X18305156, 2018.

Wright, R., Flynn, L., Garbeil, H., Harris, A., and Pilger, E.: Automated volcanic eruption detection using MODIS, Remote Sens-
ing of Environment, 82, 135–155, https://doi.org/10.1016/S0034-4257(02)00030-5, http://www.sciencedirect.com/science/article/pii/
S0034425702000305, 2002.

Yuwei, W. U., Jianqiao, H. E., Zhongming, G. U. O., and Anan, C.: Limitations in identifying the equilibrium-
line altitude from the optical remote-sensing derived snowline in the Tien Shan, China, Journal of Glaciology, 60,
1093–1100, https://doi.org/10.3189/2014JoG13J221, http://www.cambridge.org/core/journals/journal-of-glaciology/article/
limitations-in-identifying-the-equilibriumline-altitude-from-the-optical-remotesensing-derived-snowline-in-the-tien-shan-china/
6B84B734744312D483016C99C6373356, publisher: Cambridge University Press, 2014.

Zheng, W., Pritchard, M. E., Willis, M. J., Tepes, P., Gourmelen, N., Benham, T. J., and Dowdeswell, J. A.: Accelerating glacier mass
loss on Franz Josef Land, Russian Arctic, Remote Sensing of Environment, 211, 357–375, https://doi.org/10.1016/j.rse.2018.04.004,
http://www.sciencedirect.com/science/article/pii/S0034425718301494, 2018.

Zheng, W., Durkin, W. J., Melkonian, A. K., and Pritchard, M. E.: Cryosphere And Remote Sensing Toolkit (CARST) v1.0.1,
https://doi.org/10.5281/zenodo.3475693, https://zenodo.org/record/3475693#.XvSuS2hKhPZ, 2019a.

Zheng, W., Pritchard, M. E., Willis, M. J., and Stearns, L. A.: The Possible Transition From Glacial Surge to Ice Stream on Vavilov Ice
Cap, Geophysical Research Letters, 46, 13 892–13 902, https://doi.org/10.1029/2019GL084948, http://agupubs.onlinelibrary.wiley.com/
doi/abs/10.1029/2019GL084948, _eprint: https://onlinelibrary.wiley.com/doi/pdf/10.1029/2019GL084948, 2019b.